Journal Name

ARTICLE TYPE

Cite this: DOI: 10.1039/xxxxxxxxxx

Lifted graphene nanoribbons on gold: from smooth sliding to multiple stick-slip regimes

L Gigli,[a] N Manini,[b] E Tosatti,[a,c,d] R Guerra,[b,e] and A Vanossi[d,a]

Received Date
Accepted Date

DOI: 10.1039/xxxxxxxxxx

www.rsc.org/journalname

Graphene nanoribbons (GNRs) physisorbed on a Au(111) surface can be picked up, lifted at one end, and made slide by means of the tip of an atomic-force microscope. The dynamical transition from smooth sliding to multiple stick-slip regimes, the pushing/pulling force asymmetry, the presence of pinning, and its origin are real frictional processes in a nutshell, in need of a theoretical description. To this purpose, we conduct classical simulations of frictional manipulations of a 30 nm-long GNR, one end of which is pushed or pulled horizontally while held at different heights above the Au surface. These simulations allow us to clarify theoretically the emergence of stick-slip originating from the short 1D edges rather than the 2D "bulk", the role of adhesion, of lifting, and of graphene bending elasticity in determining the GNR sliding friction. The understanding obtained in this simple context is of additional value for more general cases.

Keywords: graphene, nanoribbon, stick-slip, friction.

1 Introduction

The science of nanoscale friction, a property of moving nanometer-sized interfaces widely investigated experimentally by atomic force microscopy (AFM), is progressively unveiling the detailed dissipation mechanisms in well-controlled frictional setups[1–10]. Graphene is an important actor in this quest[11–19], because its strong resilient structure makes it possible to push and slide flakes and planes once deposited on suitable well-defined surfaces[20,21]. Graphene nanoribbons (GNRs) too can be created and physisorbed on Au(111) surfaces, by means of clever in-situ molecular-assembly techniques[22,23]. Once there, they can be picked up at one extreme and forced to slide by a moving tip[24,25]. The dynamics of the GNR once dragged forward and backward (calling forward the pulling, backward the pushing, as sketched in Fig. 1) may show distinct regimes of motion depending on the lifting height, z_0. At small lifting heights ($z_0 = 1$–3 nm) there is an almost symmetric behavior between forward and backward scans, not unlike that observed experimentally for the low-lifted GNR[24]. At larger heights ($z_0 = 4$–5 nm), different stick-slip patterns and periodicities emerge with a substantial asymmetry between the two.

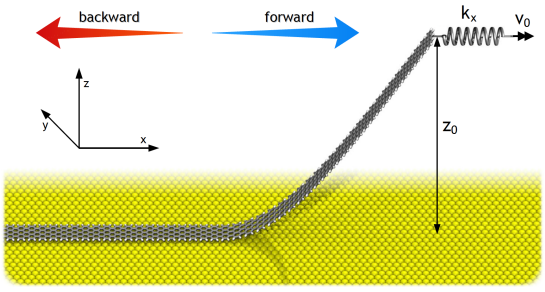

Fig. 1 Schematic description of the setup used to simulate the AFM tip lifting the GNR at one end and pulling it laterally. One side of a soft spring is attached to the lifted end of the GNR, the other side is moving at constant positive or negative velocity, thus dragging the GNR forward or backward. The height z_0 of the lifted end is kept fixed in the simulations (see Method).

The present theoretical study aims at understanding the main features of frictional dissipation in these systems.

Anticipating our final conclusions, the forward-backward symmetric frictional response at small lifting heights stems from the limited extent of elastic deformations accumulated by the GNR when pulled against an energy barrier. At increasing lifting height, the bending energy required to deform the GNR decreases and the mechanical response under driving becomes different for

[a] *International School for Advanced Studies (SISSA), Via Bonomea 265, 34136 Trieste, Italy*
[b] *Dipartimento di Fisica, Università degli Studi di Milano, Via Celoria 16, 20133 Milano, Italy*
[c] *The Abdus Salam International Centre for Theoretical Physics (ICTP), Strada Costiera 11, 34151 Trieste, Italy*
[d] *CNR-IOM Democritos National Simulation Center, Via Bonomea 265, 34136 Trieste, Italy*
[e] *Center for Complexity and Biosystems, University of Milan, 20133 Milan, Italy*

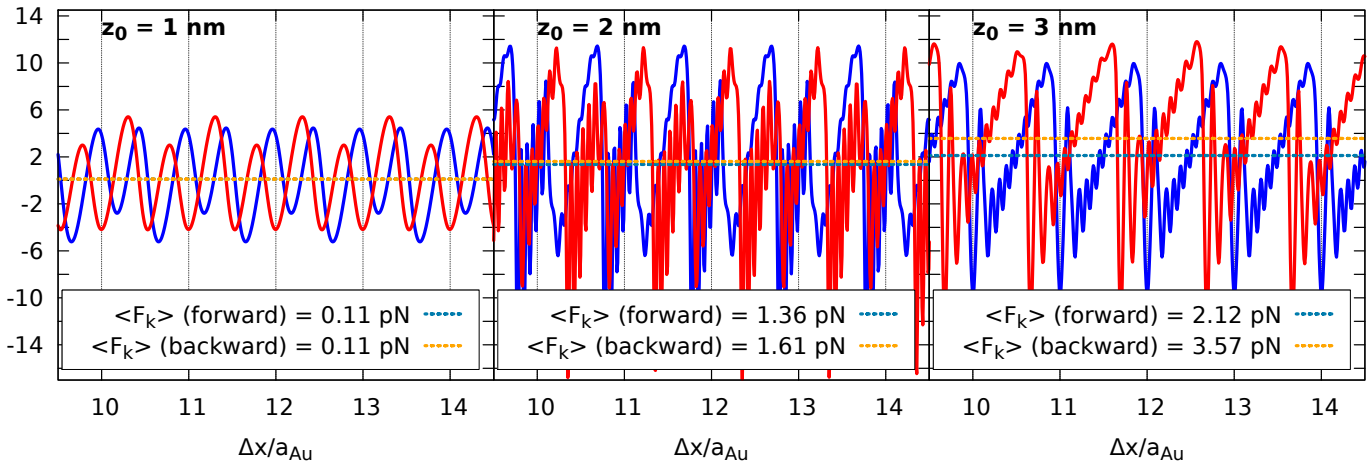

Fig. 2 Frictional force for GNR sliding at relatively small lifting heights $z_0 = 1$–3 nm. The blue and red solid curves refer to the forward and backward sliding, respectively. Dotted curves report the corresponding average frictional values.

the two opposite scan directions. Once the GNR reaches the minimum energy needed to initiate sliding (the Peierls-Nabarro barrier[26]), its dynamics starts to develop asymmetric features in the emerging stick-slip regime for forward and backward pulling. The main effects of this enhanced elastic deformation are an increased period of the stick-slip motion and the occurrence of a possible "peeling" effect in the backward trace for increasing lifting height.

Since thermal effects are always expected to be quite relevant when dealing with nanoscale systems and depinning mechanisms, we recall that the very low experimental temperature ($T = 4.8$ K)[24], excludes here a possible significant thermal contribution in the observed phenomenology.

In addition, we show that the peaks of the time-resolved frictional force traces depend critically on the effective contact length of the GNR section still adhering to the substrate. The force peak amplitudes exhibit an oscillation versus effective length of the GNR, mostly due to the imperfect compensation of the moiré superstructure at the two ends of the physisorbed part of the GNR. This effect is also related to the oscillatory behavior of the static friction force versus size reported in the past for totally adhering GNRs[27].

2 System and method

We simulate a $N = 7$ armchair GNR, consisting of a stripe of alternating triplets and pairs of carbon hexagons, of width ~ 0.7 nm and length ~ 30.2 nm, namly a factor $\simeq 5$ longer than in our reference experiment[24]. This length enables us at the same time to reproduce qualitatively the behavior of the force traces at small lifting height z_0 obtained experimentally with a much shorter GNR, and to anticipate phenomena that should come into play when the lifting height is sufficiently large ($z_0 > 5$ nm), a regime where GNRs will undergo important elastic deformations. All the edge C-atoms at the periphery of the GNR are passivated with hydrogens, in order to reproduce faithfully the experimental conditions[24], and to obtain realistic peripheral C-C bond lengths, which are sensitive to saturation effects.

The simulated GNR is deposited on an unreconstructed Au(111) surface along the R30 direction, i.e. the GNR long axis lies parallel to the Au$[-1,0,1]$ crystallographic direction[27]. The atomistic dynamics of the GNR is simulated using the LAMMPS package[28] by means of a REBO force field[29] for C-C and C-H interaction, plus 2-body C-Au and H-Au interactions of the (6-12) Lennard-Jones (LJ) type, as parametrized in Ref.[27]. In the following we refer to these energy contributions as V_{REBO} and V_{LJ}, respectively.

Starting from a fully relaxed GNR configuration, we lift progressively one end row (three C atoms) of the GNR through a fictitious ultra-hard spring ($k_z = 1.6 \cdot 10^5$ N/m), producing unilateral detachment up to a desired height $z_0 = 1$–13 nm, followed by a further relaxation in the lifted geometry. We note that the assumption of a very stiff normal spring k_z, representing experimentally the effective spring constant of the "series" of the cantilever vertical mode, of the tip apex elasticity, and of the tip-GNR bonds, allows us to better highlight the distinct dynamical behaviors of the system at almost constant values of the vertical z-coordinate. Numerical simulations with much softer k_z values (see Supplementary Information) show, anyway, equivalent tribological trends.

z_0 is defined relative to the unlifted GNR configuration. After lifting, the mean coordinate of the lifted end of the GNR, while held all the time at its fixed height z_0, is connected to a soft horizontal pulling spring ($k_x = 1.5$ N/m) and dragged forward or backward with constant velocity $v_0 = \pm 0.5$ m/s. This procedure aims at mimicking, at least qualitatively, the lateral manipulation of a GNR, as done in AFM experiments[24].

While the real-time evolution of the underlying Au substrate is not explicitly simulated, the GNR C and H atoms obey a dissipative Langevin dynamics, at zero temperature and damping parameter $\gamma = 0.01$ ps^{-1}, which prevents the externally-driven nanoribbon from heating up. We checked that the specific adopted γ value ensures a realistic relative balance of inertial and dissipative terms. The γ value does not significantly affect the qualitative outcome of the simulated tribological response within a quite broad range of values.

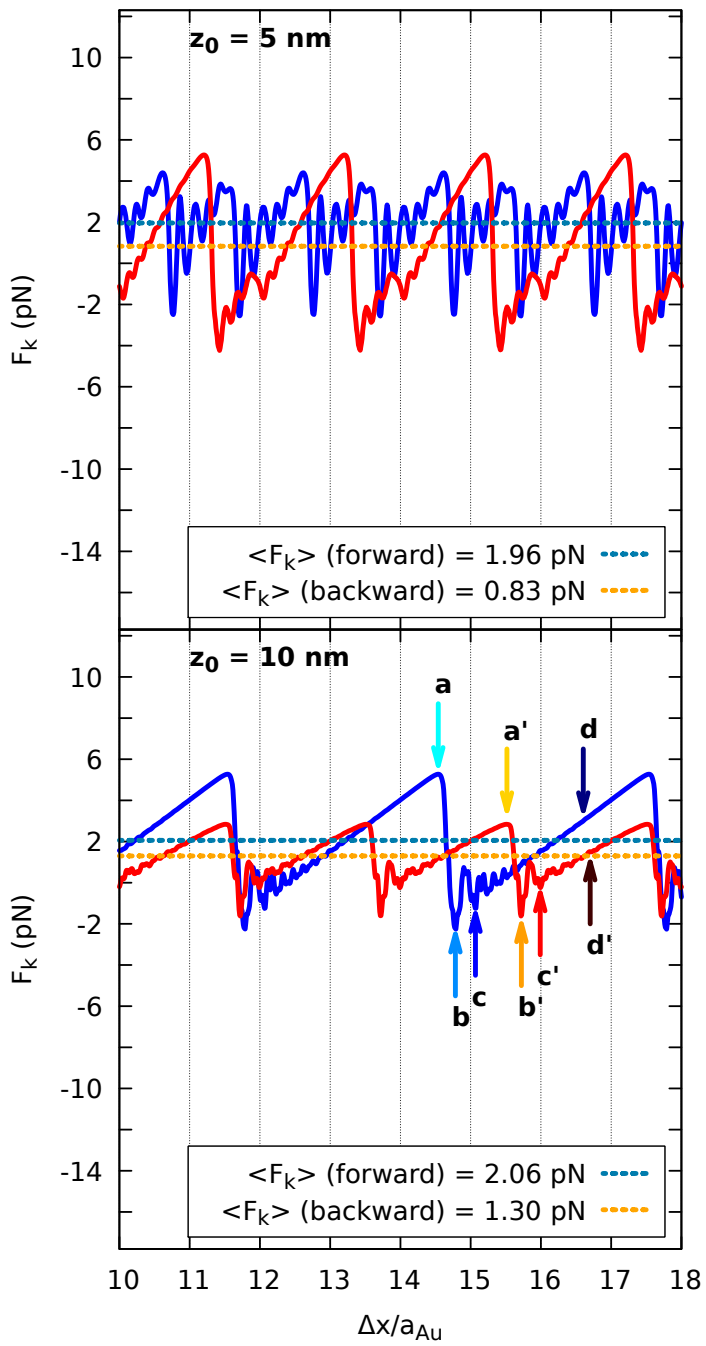

Fig. 3 Frictional force for GNR sliding at relatively large lifting heights $z_0 = 5$ and 10 nm. The blue and red solid curves refer to the forward and backward sliding, respectively. Dotted curves report the corresponding average frictional values. Arrows identify some characteristic GNR configurations during the motion at $z_0 = 10$ nm: (a) the end of the stick phase, (b) the end of the slip phase, (c) the beginning of stick, (d) half-stick. Non-primed and primed letters are for forward and backward motion, respectively. The GNR geometries for the configurations marked by arrows are reported in Fig. 4.

The equation of motion for each of the three C atoms of the lifted edge reads:

$$m_C\ddot{\mathbf{r}}_i = -m_C\gamma\dot{\mathbf{r}}_i - k_z(z_i - z_0)\hat{\mathbf{z}} - k_x(x_i - v_0t)\hat{\mathbf{x}} - \nabla_{\mathbf{r}_i}V(\mathbf{r}_i,\{\mathbf{R}_{\mu'}\}). \quad (1)$$

$\mathbf{r}_i = (x_i, y_i, z_i)$ $(i = 1,2,3)$ are the positions of the three C-atoms of the lifted edge. $\hat{\mathbf{x}}$ and $\hat{\mathbf{z}}$ the unit vectors directed along the x- and z-axis (see Fig. 1). $V(\mathbf{r}_i,\{\mathbf{R}_{\mu'}\}) = V_{\mathrm{REBO}}(\mathbf{r}_i,\{\mathbf{R}_{\mu'}\}) + V_{\mathrm{LJ}}(\mathbf{r}_i,\{\mathbf{R}_{\mu'}\})$ is the total potential energy including the interaction among all GNR particles and between particles and substrate. The equation of motion for all the other atoms with coordinates $\mathbf{R}_\mu$ is

$$m_\mu\ddot{\mathbf{R}}_\mu = -m_\mu\gamma\dot{\mathbf{R}}_\mu - \nabla_{\mathbf{R}_\mu}V(\mathbf{r}_i,\{\mathbf{R}_{\mu'}\}). \quad (2)$$

3 Results and discussion

We extract the instantaneous simulated frictional force as the elastic force that the soft pulling spring exerts on the GNR

$$F_{\mathrm{k}}(t) = 3k_x\,[v_0t - x_{end}(t)] \quad (3)$$

where $x_{end}(t) = \sum_{i=1}^{3} x_i(t)/3$ is the mean x-coordinate of the lifted end of the GNR, obtained by averaging the coordinates $x_i(t)$ of the three lifted-edge C atoms.

For each given lifting height z_0, the simulated AFM force trace is a plot of $F_{\mathrm{k}}(t)$ as a function of time, or equivalently of the displacement of the fixed-speed end of the spring $\Delta x(t) = |v_0|t$. For ease of comparison, we express this displacement in units of the lattice spacing of the gold substrate in the pulling direction, $a_{\mathrm{Au}} = 2.8838$ Å.

Discarding initial transients, Figures 2 and 3 show the steady-state simulated frictional forces for lifting heights $z_0 = 1-3$ nm, and $5-10$ nm, respectively. For a direct comparison highlighting intrinsically different features between the forward (blue solid curves) and backward (red dashed curves) traces we show the backward forces reversed in sign and plotted as a function of positive (i.e. reversed) displacements. As a consequences, the displayed force traces do not highlight here the typical dissipation frictional loop usually reported for standard AFM back-and-forth scans. At low lifting heights, $z_0 = 1-3$ nm, Fig. 2, the computed force traces for the forward and backward scans exhibit a symmetric response, as observed in experiment[24]. Note that the experimental traces also contain a long-wavelength modulation[24] due to the Au-substrate reconstruction, here neglected. At the small lifting of $z_0 = 1$ nm the sliding force oscillation reflecting the atomic corrugation on Au(111) is smooth in both directions (see Movies in Supplementary data). As a result, the average frictional force (0.1 pN) is close to zero, confirming the superlubric characteristic of the interface. We note that, due to the lattice mismatch between the GNR structure and the underneath substrate along the considered R30 direction, there exist two inequivalent good matching interface configurations, shifted almost by one half Au lattice spacing,: this condition gives rise to an approximate period doubling in the force traces.

The frictional evolution for increasing lifting height is remarkable. A first change in the dynamical response appears between 1 and 2 nm lifting. At $z_0 = 2$ nm the smooth sliding is replaced by atomic stick-slip with the same periodicity of the smooth oscillations at 1 nm. With the occurrence of this intermittent dynamics, usually marking in tribological systems the demise of superlubricity[2], we very reasonably find that friction rises by an order of magnitude. It can be noted that at the end of each slip the instan-

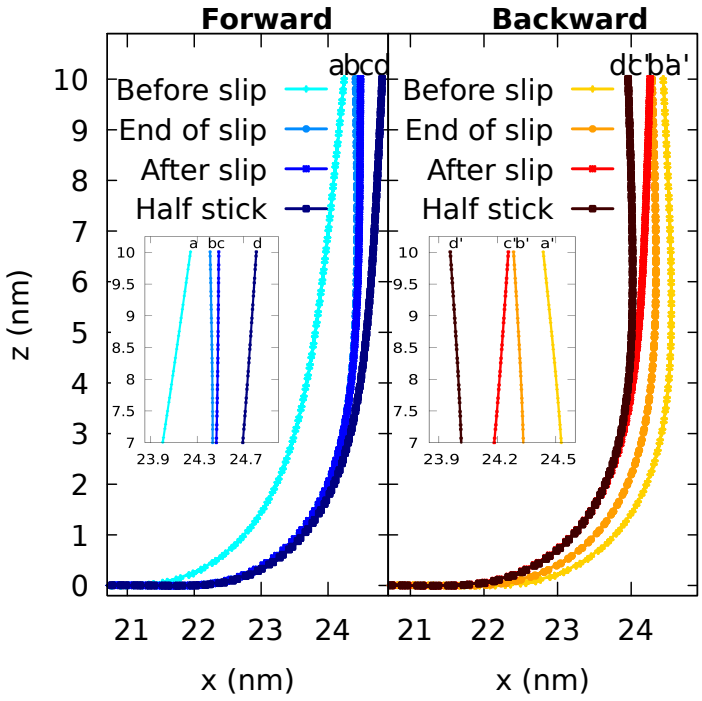

Fig. 4 The GNR lateral profile at $z_0 = 10$ nm during the forward (left panel) and backward (right panel) motion for the four successive states marked by arrows in Fig.3. The two insets help in highlighting the distinct GNR configurations near the lifted edge, during the stick-slip regime.

taneous force oscillates considerably, in both forward and backward traces, due to inertial overshooting. At higher lifting height $z_0 = 3$ a similar atomic stick slip is again observed, but without the delicate superimposed period duplication observed at smaller z_0.

A different scenario emerges for higher lifting, such as $z_0 = 5$ and 10 nm, Fig. 3. Forward and backward traces are not symmetric anymore, and multiple jumps[30] start to show up (see Movies in Supplementary data), contrasting the basically single stick-slip regime observed at small lifting. The slip distance depends quite generally on the lifting height, which controls the mechanical softness of the lifted part, and on the pulling direction. For instance, at $z_0 = 5$ nm the forward force trace is single slip, while that of the corresponding backward scan becomes double. Conversely, at $z_0 = 10$ nm the forward trace shows a stick-slip period of three lattice spacings, as opposed to two lattice spacings in the backward case.

Such asymmetric response, as we shall see, is determined by the interplay of two main effects. Firstly, forward and backward configurations imply different effective contact areas between the GNR and the substrate. Since the static friction oscillates widely with GNR contact length L_c[27], small differences in the effective contact length can lead in general to quite different static-friction thresholds. As a result, small differences in z_0 may lead to quite different dynamical friction patterns.

Secondly, as detailed in Sect. 4 below, the interplay between bending energy and adhesion differs strongly in the two pulling directions.

A first insight in the different forward and backward GNR dynamics can be obtained by examining the characteristic shape of the GNR at specific instants during the stick-slip motion. Figure 4 shows the lateral profile of the GNR in the forward and backward motion at $z_0 = 10$ nm, at four distinct instants marked by arrows in Fig. 3. The main features of the stick-slip dynamics in the forward and backward motion are very similar. Once the spring reaches the critical elongation to overcome the Peierls-Nabarro barrier (a/a'), a slip event occurs: the physisorbed section sprints forward/backwards and reaches a new pinned position (b/b'). The GNR deformation occurring at slip leads to an *increase* (in the forward motion) */decrease* (in the backward motion) of the GNR bending energy. This elastic energy is then progressively *released/absorbed* during the subsequent stick phase (c→d / c'→d').

4 Energy considerations

It is instructive to analyse how the individual energy contributions coming from the elastic bending of the GNR and from the adhesion to the substrate evolve during the stick-slip frictional dynamics. Consider for instance the motion of the GNR at large $z_0 = 10$ nm. The total GNR potential energy V is the sum of an intra-ribbon term, V_{REBO} from the C-C and C-H bonds, which controls the planar and bending stiffness, plus a second term, V_{LJ}, stemming from the C-Au and H-Au interactions which controls the adhesion of the unlifted part of the GNR. The time variation of V with respect to our reference configuration at $t = 0$, (a relaxed GNR with one lifted end), can be written as

$$\Delta V(t) = \Delta V_{\mathrm{REBO}}(t) + \Delta V_{\mathrm{LJ}}(t)\,. \tag{4}$$

For forward and backward motion, Fig. 5 compares the frictional force evolution (already displayed in Fig. 3) and that of the potential energy terms ΔV_{REBO}, ΔV_{LJ} and ΔV. Note the opposite contributions to the total GNR energy for forward and backward sliding. In the forward scan, the intra-ribbon contribution ΔV_{REBO} is negative, with an energy gain due to the decrease of GNR curvature in the detached part, as discussed in Sect. 3 above. At the same time, the system loses adhesive energy, not just because the external force works to overcome the static friction energy barrier which blocks the sliding, but mainly because the physisorbed section shortens in length as the GNR end is pulled forward, causing an increase of ΔV_{LJ}. This is also made evident in the zoomed-in GNR z-profile of Fig. 6) Exactly the opposite occurs for backward sliding, where ΔV_{REBO} is positive, owing to the curvature increase of the detached part, whereas ΔV_{LJ} is negative reflecting a corresponding improvement of adhesion due to an increased contact length L_c (see again Fig. 6). For completeness, we note that, at even larger z_0 values, the backward-driven GNR may initiate to peel off the Au surface during the stick phase, thus starting a decrease in the ΔV_{LJ} adhesive contribution.

There is a clear correspondence between the energy evolution described above and the lifted nanoribbon geometry. Figure 6 compares the shape profile $z = z(x)$ of the GNR near the detachment point, just before the slip either forward or backward. By comparison with the relaxed, static shape (zero force), the curvature and the physisorbed section of the GNR are respectively smaller in the forward case, and larger in the backward case.

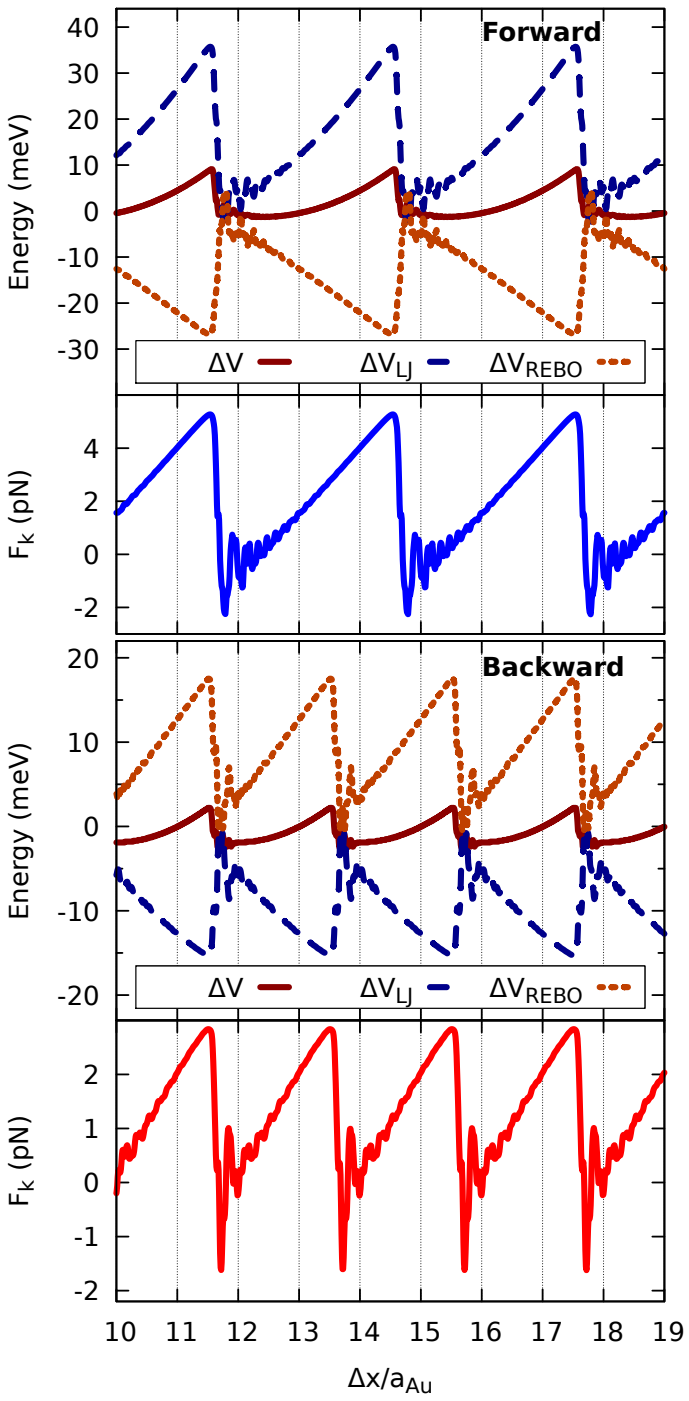

Fig. 5 Comparison between the frictional force and the variation of the elastic intra-ribbon V_{REBO} and adhesive ribbon-substrate V_{LJ} contributions to the GNR total energy in the stick-slip motion at $z_0 = 10\,\mathrm{nm}$.

5 Role of the ribbon short edge and uncompensated moiré pattern

As was observed in our previous study of the fully adhering – non-lifted – GNRs[27], the 2D "bulk" of the GNR/Au(111) interface is incommensurate and structurally lubric ("superlubric"). Like in other superlubric systems, the static friction – the minimal force required to set the interface into sliding motion – does not grow

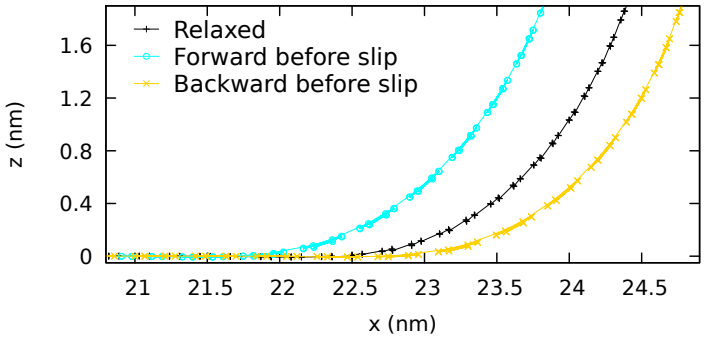

Fig. 6 GNR lateral profile close to the detachment region in the forward (cyan line) and backward motion (yellow line) just before the slip. The configuration of the relaxed GNR at rest (black line) is included as reference.

(on average) as much as the contact area. Specifically, for a non-lifted GNR, the static friction oscillates around a fairly constant mean value as a function of the nanoribbon length[27]. This indicates that the edges, here the short ones, are mostly responsible for pinning – a feature similarly found in incommensurate rare-gas islands deposited on metal surfaces[31] and in twisted bilayer graphene[32]. The strong oscillation of the static friction F_{s} around the constant average trend as a function of the GNR length is related to the "uncompensated" moiré pattern near the GNR ends, i.e. the residual of L_c divided by the moiré-pattern wavelength. This friction oscillation may involve variations in F_{s} comparable with the average[32]. This appears to be the case also with lifted GNRs, where the effective contact length L_{eff}, defined below, varies as a function of z_0 and changes dynamically in time.

By lifting the GNR at successively increasing heights, the effective contact length L_{eff} will change, giving rise to minima/maxima of the static friction force. We define the effective contact length L_{eff} of a lifted GNR by dividing V_{LJ} by the same quantity per unit length of an infinite-length simulated GNR with periodic boundary conditions, V_{LJ}^{∞}:

$$L_{\mathrm{eff}}(z_0,t) = \frac{V_{\mathrm{LJ}}(z_0,t)}{V_{\mathrm{LJ}}^{\infty}}\,, \tag{5}$$

where $V_{\mathrm{LJ}}(z_0,t)$ is the total interaction energy between the GNR and the substrate at the lifting height z_0 and at time t. It turns out that for lifting heights between $z_0 = 7.5\,\mathrm{nm}$ and $z_0 = 12.5\,\mathrm{nm}$ we cover one complete period of the static friction[27]. Figure 7 shows the force traces corresponding to lifting heights $z_0 = 7.5$, 9.9, and 12.5 nm, along with the corresponding change in time of the effective contact length $L_{\mathrm{eff}}(z_0,t)$ of Eq. (5). $z_0 = 7.5$ and 12.5 nm correspond to expected local maxima of the oscillating static friction versus effective size. $z_0 = 9.9$ represents an expected local static-friction minimum, As expected, the peaks in F_{k} and the mean friction forces are larger at lifting heights that correspond to the expected local maxima of static friction, namely $z_0 = 7.5\,\mathrm{nm}$ and $z_0 = 12.5\,\mathrm{nm}$, than at $z_0 = 9.9\,\mathrm{nm}$.

For a grid of lifting heights z_0, Fig. 8 reports the maximum force $F_{\mathrm{k}}^{\mathrm{max}}$ obtained from the peaks just before slip. These values exclude an initial transient and are evaluated once a steady stick-slip regime is established. We report these data, rather than as

functions of z_0, as functions of the effective contact length $L_{\rm eff}$ for that height. The best-fitting sinusoids of the form

$$F_{\rm k}^{\rm max}(L) = \alpha + \beta \sin\left(\frac{2\pi L}{\lambda_m} - \delta\right), \qquad (6)$$

for both the forward and backward motion, are also drawn as reference. α, β, λ_m, δ are fitting parameters. The values and the $\lambda_m = 4.86$ nm period oscillation of the lifting-dependent maximum force compares reasonably well with the established static friction trend as a function of the non-lifted GNR length [27], reported in the lower panel of Fig. 8. Somewhat larger in magnitude, both forward and backward maximum forces share the same oscillation as the static friction of the non-lifted GNR with length equal to the effective lifted GNR length $L_{\rm eff}$. This result further confirms that the uncompensated, edge-related, part of the moiré pattern determines the magnitude of the maximum kinetic-friction force before slip.

Figure 8 compares the maximum kinetic friction $F_{\rm k}^{\rm max}$ with the static friction $F_{\rm s}$ obtained for fully adhering GNRs [27]. For a given system in the underdamped regime, the two quantities should match in the limit of vanishing driving velocity v_0. At finite velocity it is generally expected that $F_{\rm s} > F_{\rm k}^{\rm max}$, with static friction always exceeding dynamic one. Here we observe the opposite. This might look counterintuitive, as one might expect a larger friction for fully adhering GNRs. However, as pointed out above, static friction is dominated by the two GNR short-ends in this superlubric system. The two short-edges are equivalent in the unlifted case, and are responsible for the frictional oscillations as a function of L_c [27]. By contrast, in the case of lifted GNR the bending at the leading edge produces a termination which is strongly inequivalent to that of the trailing edge. As a result, cancellation of the lateral forces acting on the two ends is more problematic, yielding generally an overall larger friction.

It is also worth asking if GNRs might show any tendency to peel off the substrate when driven backward at large lifting heights. As seen in Figures 5 and 6, the backward stick-slip motion is accompanied by an *increase* of adhesion in the stick state, while a *decrease* of adhesion is seen in the forward motion. In Figure 7, $z_0 = 9.9$ nm, this fact is confirmed by the increase of $L_{\rm eff}$ in the stick state of the backward motion. In these cases no tendency to peel off is registered. In contrast, at a lifting height of 12.5 nm, we notice that in the backward motion the adhesive length increases up to a maximum and then decreases again with a sort of parabolic trend. This indicates that the spring initially pushes the physisorbed atoms adjacent to the bent GNR section down in closer contact with substrate, promoting an increased adhesion. Once the extension of the driving spring is sufficiently large, the GNR starts to detach from the substrate, causing a loss of adhesion. This analysis shows that, depending on the lifting height z_0 and the precise value of the static friction barrier at that height, the GNR can indeed start to peel off from the substrate. In all simulated cases, as backward pulling continued, a slip event would release the bending stress before the peeling instability would fully develop and lead the GNR to a complete peel off. As a general rule, peeling is more pronounced for those combinations of z_0 and GNR length leading to those $L_{\rm eff}$ producing the largest possible static friction threshold, and generally for larger lifting height, because of the softer GNR elasticity and greater mechanical advantage.

6 Conclusions

We have investigated the dynamical friction of lifted graphene nanoribbons on a Au(111) substrate by means of non-equilibrium molecular-dynamics simulations. Mimicking the experimental setup of Kawai et al. [24] we reproduce and interpret the observed frictional regimes of the GNR as a function of the lifting height z_0. For increasing z_0, we predict a remarkable transition from smooth sliding to atomic stick-slip, characterized initially by single slips, and then by multiple slips at larger heights. Specifically, the periodicity of the stick-slip dynamics is dominated by the bending elasticity of the GNR, which enables larger slip distances at larger heights. The augmented softness, introduced by bending of the GNR as z_0 increases, plays opposite roles for the two driving directions, decreasing (forward) and increasing (backward) the GNR/substrate adhesion. The lifting-dependent amplitude of the instantaneous friction force is not a "bulk" feature, and is entirely determined by the short edges of the GNR – in the lifted case as well as in the non-lifted case.

We find an oscillation of friction with lifting height. This in turn is related, via identification of an effective GNR contact length of the physisorbed GNR section, to the moiré-pattern lack of compensation close to the edges, qualitatively similar but quantitatively different to that occurring in the static friction of unlifted GNRs [27]. Past experiments on lifted GNR sliding [24] have not yet explored the new regime which we describe here, essentially due to the relatively small length of the GNR used there (6.28 nm only), whereby the GNR lifted at 5 nm was almost completely detached from the Au-substrate, very nearly peeled off. Our much longer – 30 nm – simulated GNR, only approaches peeling at lifting heights larger than ~ 10 nm, as shown by the time evolution of the effective contact length. A more precise evaluation of this critical lifting height would probably require a further refinement of the modeling setup, taking also into account the mobility of the underneath gold substrate.

Present predictions about the sliding should be borne out by future experiments, hopefully on longer GNRs, as well as on more general physisorbed flakes of graphene and other 2D materials. In these systems, it should be possible to find, for increasing lifting heigthts, a transition from smooth sliding to stick-slip, the asymmetric forward/backward friction, and a peel-off instability.

Acknowledgments

We acknowledge useful discussions with E. Meyer, E. Gnecco and A. Benassi. Work in Trieste was carried out under ERC Grant 320796 MODPHYSFRICT. The COST Action MP1303 is also gratefully acknowledged.

Conflicts of interest

There are no conflicts to declare.

References

1 Krim J 2012 *Adv. Phys.* **61** 155

2 Vanossi A, Manini N, Urbakh M, Zapperi S and Tosatti E 2013 *Rev. Mod. Phys.* **85** 529

3 Park J Y and Salmeron M 2014 *Chem. Rev.* **114** 677

4 Manini N, Braun O, Tosatti E, Guerra R and Vanossi A 2016 *J. Phys.: Condens. Matter* **28** 293001

5 Manini N, Mistura G, Paolicelli G, Tosatti E and Vanossi A 2017 *Adv. Phys. X.* **2** 569

6 Manini N, Braun O and Vanossi A 2015 *Nanotribology: Nonlinear Mechanisms of Friction* (Springer, Berlin) pp 175; DOI:10.1007/978–3–319–10560–4_10

7 Dietzel D, Ritter C, Mönninghoff T, Fuchs H, Schirmeisen A and Schwarz U D 2008 *Phys. Rev. Lett.* **101** 125505

8 Brndiar J, Turanský R, Dietzel D, Schirmeisen A and Štich I 2011 *Nanotechnology* **22** 085704

9 Dietzel D, Feldmann M, Schwarz U, Fuchs H and Schirmeisen A 2013 *Phys. Rev. Lett.* **111** 235502

10 Mougin K, Gnecco E, Rao A, Cuberes M T, Jayaraman S, McFarland E W, Haidara H and Meyer E 2008 *Langmuir* **24** 1577

11 Filleter T, McChesney J L, Bostwick A, Rotenberg E, Emtsev K V, Seyller Th, Horn K and Bennewitz R 2009 *Phys. Rev. Lett.* **102** 086102

12 Lee C, Li Q, Kalb W, Liu X-Z, Berger H, Carpick R W and Hone J 2010 *Science* **328** 76

13 Berman D, Erdemir A and Sumant A V 2014 *Mater. Today* **17** 31

14 Choi J S, Kim J S, Byun I S, Lee D H, Lee M J, Park B H, Lee C, Yoon D, Cheong H, Lee K H, Son Y W, Park J Y and Salmeron M 2011 *Science* **333** 607

15 Feng X, Kwon S, Park J Y and Salmeron M 2013 *ACS Nano* **7** 1718

16 Kwon S, Ko J-H, Jeon K-J, Kim Y-H and Park J Y 2012 *Nano Lett.* **12** 6043

17 Bonelli F, Manini N, Cadelano E and Colombo L 2009 *Eur. Phys. J. B* **70** 449

18 Gao W and Tkatchenko A 2015 *Phys. Rev. Lett.* **114** 096101

19 Klemenz A, Pastewka L, Balakrishna S G, Caron A, Bennewitz R and Moseler M 2014 *Nano Lett.* **14** 7145

20 Dienwiebel M, Verhoeven G S, Pradeep N, Frenken J W M, Heimberg J A and Zandbergen H W 2004 *Phys. Rev. Lett.* **92** 126101

21 Filippov A E, Dienwiebel M, Frenken J W M, Klafter J and Urbakh M 2008 *Phys. Rev. Lett.* **100** 046102

22 Cai J, Ruffieux P, Jaafar R, Bieri M, Braun T, Blankenburg S, Muoth M, Seitsonen A, Saleh M, Feng X, Müllen K and Fasel R 2010 *Nature* **466** 470

23 Lingxiu C, Li H, Hui S W, Haomin W, Shujie T, Chunxiao C, Hong X, Lei L, Hui X, Tianxin L, Tianru W, Daoli Z, Lianwen D, Ting Y, Xiaoming X and Jiang M 2017 *Nature Comm.* **8** 14703

24 Kawai S, Benassi A, Gnecco E, Söde H, Pawlak R, Feng X, Müllen K, Passerone D, Pignedoli C A, Ruffieux P, Fasel R and Meyer E 2016 *Science* **351** 957

25 Kawai S, Koch M, Gnecco E, Sadeghi A, Pawlak R, Glatzel T, Schwarz J, Goedecker S, Hecht S, Baratoff A, Grill L and Meyer E 2014 *Proc. Nat. Ac. Soc.* **111** 3968

26 Floría L and Mazo J 1996 *Adv. Phys.* **45** 505

27 Gigli L, Manini N, Benassi A, Tosatti E, Vanossi A and Guerra R 2017 *2D Mater.* **4** 045003

28 Plimpton S 1995 *J. Comput. Phys.* **117** 1

29 Brenner D W, Shenderova O A, Harrison J A, Stuart S J, Ni B and Sinnott S B 2002 *J. Phys.: Condens. Matter* **14** 783

30 Medyanik S, Liu W K, Sung I H and Carpick R W 2006 *Phys. Rev. Lett.* **97** 136106

31 Varini N, Vanossi A, Guerra R, Mandelli D, Capozza R and Tosatti E 2015 *Nanoscale* **7** 2093

32 Koren E and Duerig U 2016 *Phys. Rev. B* **94** 045401

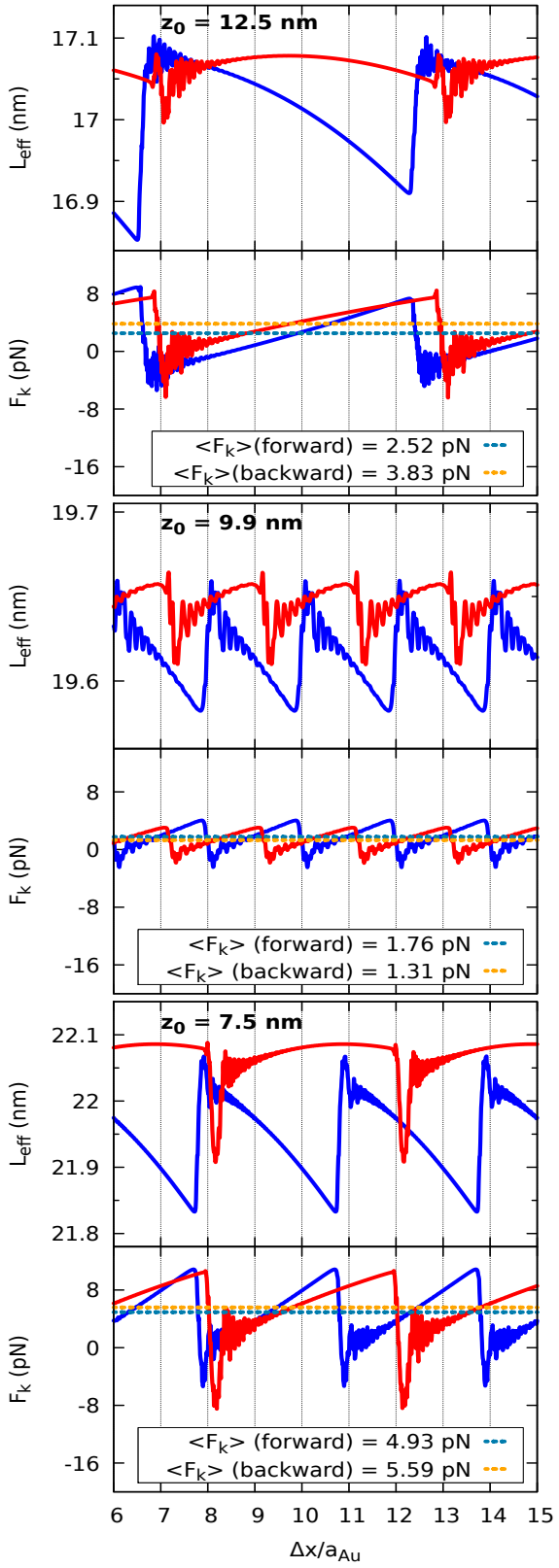

Fig. 7 Comparison between the friction-force traces for three large lifting heights, $z_0 = 7.5,\ 9.9$ and 12.5 nm, and the change of the effective instantaneous contact length $L_{\rm eff}$ between the GNR and the substrate. As previously, blue and red solid curves refer to forward and backward sliding, respectively, and dotted curves report the corresponding average values.

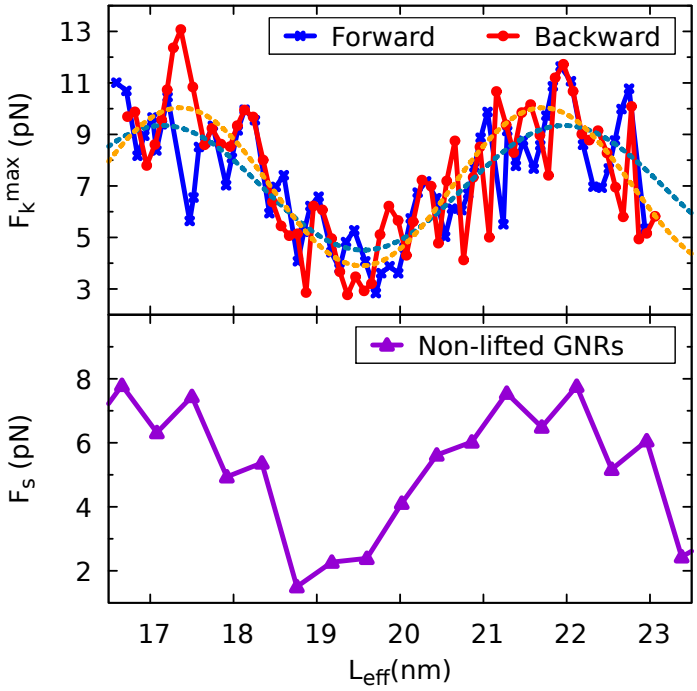

Fig. 8 Comparison between the static friction force of non-lifted GNRs[27] (lower panel), and the maximum kinetic force (upper panel), as a function of the effective contact length $L_{\rm eff}$, varied by repeating the simulations for many lifting heights z_0. The dotted cyan and orange lines are the corresponding best fitting curves of Eq. (6) to the $F_{\rm k}^{\rm max}$ data.